Type of the Paper (Article, Review, Communication, etc.)

Rapid, Simple and Inexpensive Fabrication of Paper-based Analytical Devices by Parafilm® Hot Pressing

Surasak Kasetsirikul [1,2], Kimberley Clack [1,3], Muhammad J.A. Shiddiky [1,3], and Nam-Trung Nguyen [1,*]

[1] Queensland Micro- and Nanotechnology Centre (QMNC), Griffith University, Nathan Campus, QLD 4111, Australia
[2] School of Engineering and Built Environment (EBE), Griffith University, Nathan Campus, QLD 4111, Australia
[3] School of Environment and Science (ESC), Griffith University, Nathan Campus, QLD 4111, Australia
* Correspondence: nam-trung.nguyen@griffith.edu.au

Abstract: Paper-based analytical devices have been substantially developed in recent decades. Many fabrication techniques for paper-based analytical devices have been demonstrated and reported. Herein we report a relatively rapid, simple, and inexpensive method for fabricating paper-based analytical devices using parafilm hot pressing. We studied and optimized the effect of the key fabrication parameters, namely pressure, temperature, and pressing time. We discerned the optimal conditions, including pressure of 3.8 MPa (3 tons), temperature of 80°C, and 3 minutes of pressing time, with the smallest hydrophobic barrier size (821 μm) being governed by laminate mask and parafilm dispersal from pressure and heat. Physical and biochemical properties were evaluated to substantiate the paper functionality for analytical devices. Wicking speed in the fabricated paper strips was slightly slower than that of non-processed paper, resulting from reducing paper pore size. A colorimetric immunological assay was performed to demonstrate the protein binding capacity of the paper-based device after exposure to pressure and heat from the fabrication. Moreover, mixing in two-dimensional paper-based device and flowing in a three-dimensional counterpart were thoroughly investigated, demonstrating that the paper device from this fabrication process is potentially applicable as analytical devices for biomolecule detection. Fast, easy, and inexpensive parafilm hot press fabrication presents an opportunity for researchers to develop paper-based analytical devices in resource-limited environments.

Keywords: Paperfluidics; Parafilm; Paper-based Analytical Devices

1. Introduction

Paper-based analytical devices or paperfluidic devices have attracted enormous attention in the past few decades. They demonstrated the possibility of being cost-effective, biodegradable, and used as platforms for point-of-care diagnostic devices [1-3]. Following the emergence of paper-based microfluidic technologies established by the Whiteside group in 2007 [4], many studies indicated the resilience of paper-based devices in food industry, environmental science, and medical diagnostics [1-3,5,6]. The basic principle behind paper-based technology is making paper both hydrophobic and hydrophilic, so that flow and biological assay properties can be handled within a single device. The paper-based fabrication process can be classified into two main steps: (i) deposition of patterned hydrophobicity via photolithography [7,8], wax plotting [9], polymer or wax printing [10,11], and other deposition methods [12-14], and (ii) removing hydrophobic material to get the final pattern such as inkjet etching [15], plasma etching [16], chemical wet etching [17], or laser treatment [18,19]. However, some fabrication methods involve harsh chemicals such as Tetramethyl orthosilicate (TMOS), which may be left on the paper, and inhibit the biochemical reaction [17]. In addition, some of the fabrication steps require precise and expensive machines such as laser treatment [1,6,20]. Some other fabrication methods are

Preprints (www.preprints.org) | NOT PEER-REVIEWED | Posted: 3 December 2021 doi:10.20944/preprints202112.0046.v1

simple and inexpensive. However, they yield low resolution and low reproducibility [5,20,21].

To solve the issues concerning chemical usage and low reproducibility, alternative methods and materials are required. Parafilm, which is a thermoplastic made from wax and polyolefin, was commonly used in wet laboratories. Dunfield et al. reported in 2012 the first attempt to melt parafilm onto the paper by incorporating pressure and heat [22]. They suggested that polymer film can prevent the melted parafilm from getting into the paper as it provides a hydrophobic area. Nonetheless, there is no further and detailed study on the relation of fabrication parameters for analytical applications. Yu et al. fabricated a 2D and 3D paper-based analytical device with photolithography and embossing of Parafilm [23]. However, this fabrication process required multiple steps and special equipment for lithography, which took around 30 – 40 minutes to make a device. Recently, Kim et al. studied the use of low-temperature ranges to infuse parafilm into the paper and laser ablation to remove parafilm infused paper for fluidic channels [19]. This method can create a microchannel down to 150 μm, depending on the resolution of laser ablation. Nevertheless, this fabrication method required specific and delicate equipment.

Despite the recent advancements in paper-based analytical devices, no previous studies have investigated the specific relationship between fabrication parameters such as temperature, pressure and pressing time. Herein, we optimize these parameters and their relationship to develop a simple and inexpensive analytical device for detecting biological targets via colorimetric technique. To the best of our knowledge, this proof-of-concept analytical device is to date the only device prepared by the parafilm hot pressing method. Parafilm hot pressing allows for the penetration of parafilm into the paper and represents a rapid, simple, and inexpensive method for fabricating a paper-based device. The technique requires only polymer film, parafilm, paper, and a hot press to fabricate a paper-based device. The entire process takes only 5 - 10 min for two steps: cutting and pressing, resulting in a cost of less than 0.01 USD per device. We studied the effect of temperature (60 –90°C), pressure (2.5 – 5.1 MPa), and pressing time (1-5 min) to obtain the optimal fabrication parameters. To demonstrate the functionality of the paper, we investigated the physical and biochemical properties after fabrication using wicking, 2D and 3D mixing and colorimetric immunological assay.

2. Materials and Methods

2.1 Materials and Chemicals

The material used for the device in our study is chromatography filter paper (CHR). Parafilm (Bemis Company, UK) was used to make the paper hydrophobic. A gloss laminate pouch with 80-μm thickness serve as a patterning mask for the front and back support during the fabrication process. For the colorimetric immunological assay, rabbit monoclonal anti-human CD9 (rabbit anti-CD9, ab92726, Abcam, UK) and Goat anti-rabbit IgG (anti-rabbit IgG, ab6721, Abcam, UK) were conjugated with HRP using an HRP-conjugation kit (ab102890, Abcam, UK). 3,3′,5,5′-tetramethylbenzidine substrate solution (TMB, 002023, Thermo Fisher Scientific, Germany) was used to employ the colorimetric immunological assay, facilitated by the HRP/TMB reaction. Bovine Serum Albumin (BSA, A1595, Sigma Aldrich, USA) was used to block the sensor surface to minimize the background signal due to non-specific binding. For mixing applications, 0.1 M Sodium hydroxide solution (SL178, Chem-Supply Australia) and 1% Phenolphthalein in ethanol (FE0496G100, Scharlau, Spain) were used as a mixing indicator. Four food color dyes (Queens, Australia) consisting of red, yellow, green, and blue were mixed with DI water (MilliQ, Merck) to obtain a 10% by volume ratio to illustrate the 3D paperfluidic channels.

2.2 Fabrication parameter study

Parafilm is a translucent, flexible film composed of waxes and polyolefin. Parafilm becomes soft and adhesive at a temperature between 54 – 66 °C [23]. Parafilm can be infused into the paper matrix by applying a given pressure and temperature [19,22]. Parafilm can be melted and permeated into paper through a patterning mask. The laminate

Preprints (www.preprints.org) | NOT PEER-REVIEWED | Posted: 3 December 2021 doi:10.20944/preprints202112.0046.v1

film was designed by CorelDraw software (CorelDRAW2019, Corel Corporation Inc, Canada) and cut by a laser engraving machine (Rayjet 50 Laser Engraver, Rayjet, Australia). CHR was prepared and stacked with parafilm, laminate film masks, and supports, Figure 1. Subsequently, the paper stack was covered with an aluminum foil and placed into a hot press machine (Specac, UK). To optimize the fabrication parameters for paper-based analytical devices, the permeation of parafilm into the paper by combining the three parameters: pressure (2.5 – 5.1 MPa), temperature (60 – 90°C), and pressing time (1 – 5 minutes).

2.3 Hydrophobic barrier resolution

The paper channel was patterned and determined by the laminate pattern mask, depending on the resolution of the laser engraving machine. Therefore, we first investigated the resolution of the hydrophobic barrier after depositing parafilm into the paper. The pattern was designed to determine the smallest hydrophobic structure with optimal fabrication parameters (Figure 2a). Since the laser beam provides the heat needed to melt the polymer film and cut the materials, we investigated the actual size of a single cut line. The mask was designed to create a hydrophobic barrier between two straight channels as shown in Figure 2a and defined as "no gap" condition. We investigated gap size ranging from 100 to 300 μm for the hydrophobic barrier between two straight channels. Two food dye colors were added to visualise the actual paper straight channel area and evaluate the quality of the hydrophobic barrier.

2.4 Physical and biochemical properties of the paper

2.4.1 Flowing characteristic

Pressure and heat generated during the fabrication process may affect the wicking behavior in the paper strips, so we investigated the flowing characteristics between fabricated and original paper strips. The paper strip was prepared with a laser cutting machine, with a width of 2 mm, 4 mm, and 6 mm. The capillary rise experiment setup was adapted from our previous study [24]. Briefly, the paper was vertically positioned with a customized acrylic stand. The dye solution was loaded into the liquid reservoir below the paper strip. The fluid wicking up to the paper strip was recorded, processed, and quantified using MATLAB to determine the relationship between the distance of the liquid front and time.

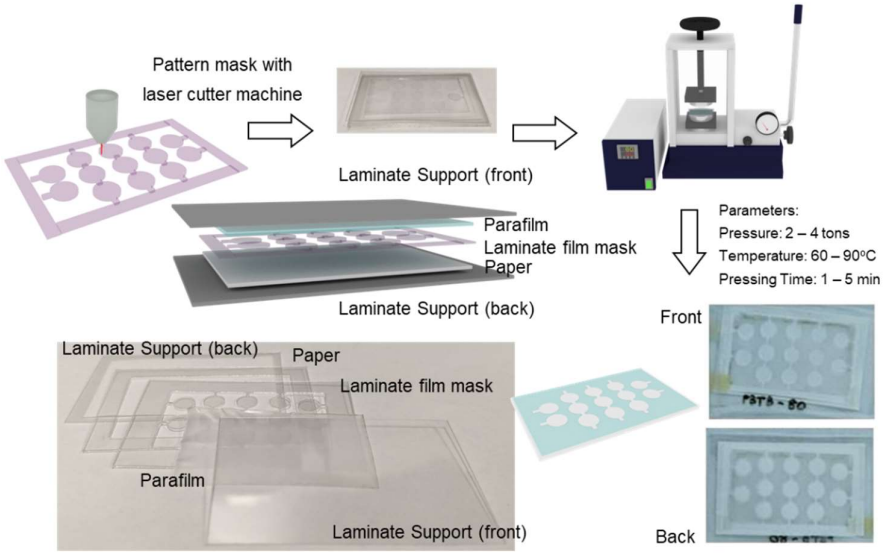

Figure 1 Schematic diagram of the fabrication process. The parafilm and patterning laminate film were placed above the paper layer, then covered with front and back laminate films and aluminum foil before placed in a hot press machine.

Preprints (www.preprints.org) | NOT PEER-REVIEWED | Posted: 3 December 2021 doi:10.20944/preprints202112.0046.v1

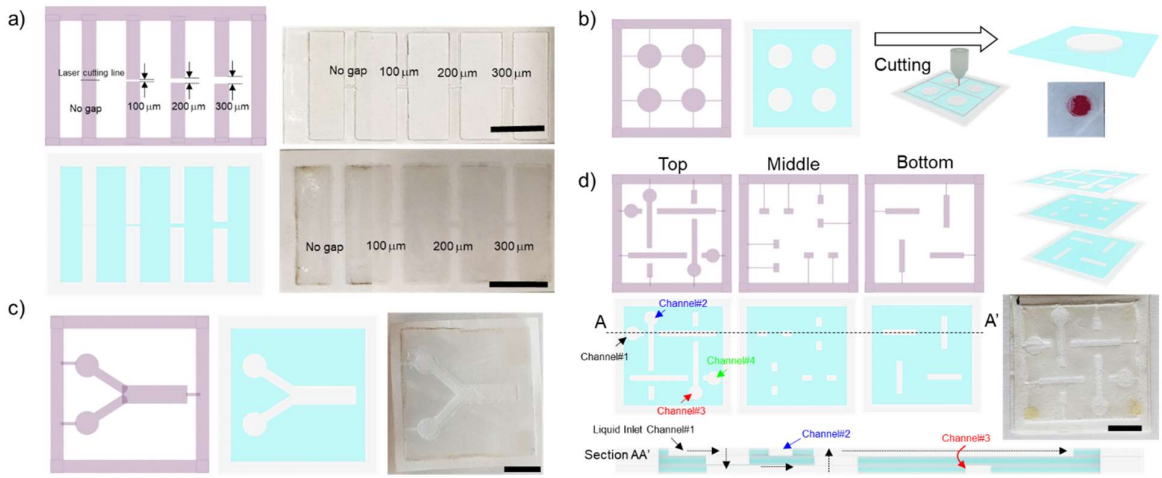

Figure 2 Laminate film for patterning masks formed with the laser cutting machine: (a) The pattern for the investigation of hydrophobic barrier resolution; (b) The pattern for the paper-based colorimetric sandwich immunological assay; (c) The pattern for mixing in the 2D analytical paper-based device; (d) The pattern for the flow in the 3D paper-based device and cross-sectional view for illustrating the 3D paper channel. Scale bar shown as 1 cm.

2.4.2 Colorimetric sandwich immunological assay

The colorimetric sandwich immunological assay demonstrates that heat and pressure from the fabrication process are compatible with the protein binding capacity on the paper matrix. The laminate film was cut into 5-mm diameter patch with support, Figure 2b. Subsequently, the paper was cut into individual devices. We employed the HRP/TMB reaction to illustrate the colorimetric assay. In the presence of HRP, TMB is oxidized, changing from colorless to a blue color complex. Briefly, the paper was coated with 5 μL of 0.1 mg/mL rabbit anti-human CD9, with subsequent blocking with 2% BSA. 3 μL of 1 μg/mL of Goat anti-rabbit IgG conjugated with HRP was added to make a sandwich immunoassay. We performed an analytical assay with and without coating rabbit anti-human CD9. The results were recorded with the setup adapted from our previous study at 20th min [25].

2.5 2D and 3D paperfluidic devices

2.5.1 Mixing in the two-dimensional paperfluidic device

We investigated mixing on a two-dimensional (2D) paper-based device. The laminate film was cut to have two inlets and a straight channel, Figure 2c. The hydrophilic channel on the paper is defined by the patterning mask. For characterization of the mixing process, 10 μL of 0.1 M Sodium Hydroxide and 10 μL of phenolphthalein solution were dropped on the left and right inlets, respectively. After mixing with the alkaline solution, the color of phenolphthalein changes from colorless to dark pink. The dark pink color developed in the straight channel confirms the mixing capability in the paper-based device.

2.5.2 Flow in a three-dimensional paperfluidic device

We also demonstrated fluid flow in the three-dimensional (3D) paper-based device. The paper device was separated into three layers, Figure 2d. Each paper layer was fabricated with the optimized conditions and then assembled together using adhesive. The different dye solutions were wicked through the straight channel between layers and demonstrate the 3D flow configuration. The food dye is expected to keeps its color at the end of the channel because the patterned hydrophilic channels do not intersect and cross contaminate each other.

2.6 Data acquisition and quantification

Images of the device were captured by the camera and evaluated with ImageJ (NIH, USA). For colorimetric quantification, the image was imported and processed with

Preprints (www.preprints.org) | NOT PEER-REVIEWED | Posted: 3 December 2021 doi:10.20944/preprints202112.0046.v1

MATLAB. First, the region of interest (ROI) was cropped. Next, the ROI pixel values were split into red, green and blue channels. Next, the mean grey value of RGB_{value} was calculated as:

$$RGB_{value} = \sqrt{(R - R_0)^2 + (G - G_0)^2 + (B - B_0)^2}, \quad (1)$$

where *R*, *G*, and *B* are the mean grey values from images for red, green, and blue channels, respectively. The mean grey values from the white background are defined as R_0, G_0 and B_0, which are red, green, and blue channel values, respectively.

3. Result and Discussion

3.1 Optimization of fabrication parameters

3.1.1 Effect of temperature

The temperature was varied in the range of 60 °C to 90 °C to optimize the temperature during fabrication. Maintaining the pressure at 2.5 MPa and 1 minute of pressing time, we found that the parafilm can be melted at a relatively high temperature and can penetrate through the paper, Figure 3a. We observed that at 60°C, parafilm could not adhere to the paper. Parafilm can permeate into the paper at temperatures of 70 °C and 80 °C, but it does not fully penetrate the paper as observed from the back, where the parafilm cannot be seen. At a temperature of 90 °C, parafilm was fully permeated into the paper. Nevertheless, if the pressure and pressing time are increased, a high temperature can result in over-permeation, Figure 3b. Providing the pressure of 5.1 MPa and 5 minutes of pressing time, parafilm at 60 °C still cannot permeate into the paper even at a higher pressure and longer pressing time. At temperatures of more than 80 °C, parafilm can fully penetrate the paper matrix, but the working area defined by the patterning mask became smaller due to overflow. In conclusion, the temperature in hot press fabrication plays a role in melting the parafilm. With the correct pressure and pressing time, the parafilm could successfully permeate into the paper.

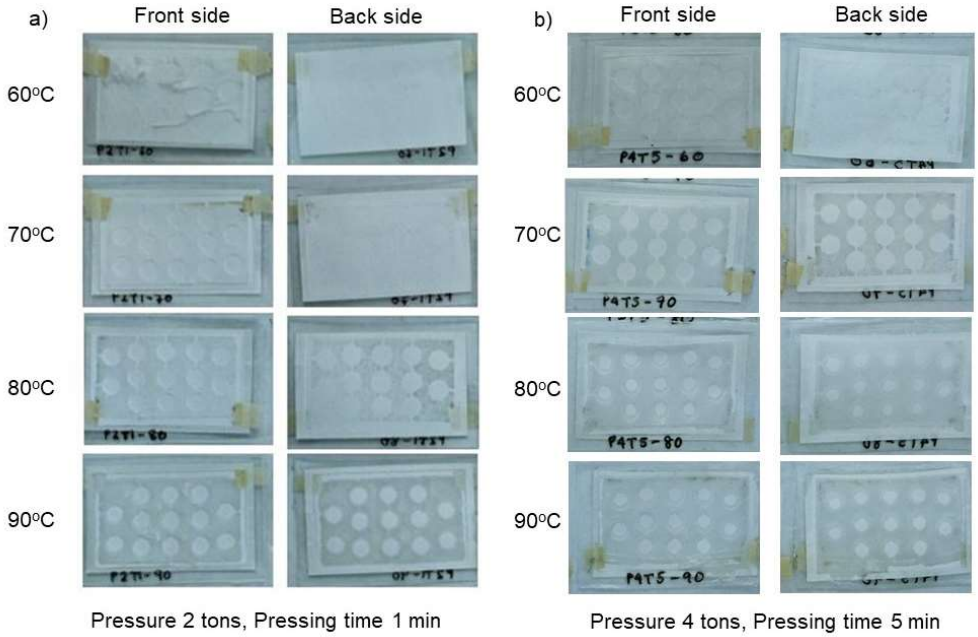

Figure 3 Effect of temperature: (a) Under a pressure of 2.5 MPa (2 tons) and 1 min pressing time; (b) Under a pressure of 5.1 MPa (4 tons) and 5 min of pressing time. The temperature was varied from 60 to 90°C (left column shows the front side, right column shows the back side).

3.1.2 Effect of pressure

Preprints (www.preprints.org) | NOT PEER-REVIEWED | Posted: 3 December 2021 doi:10.20944/preprints202112.0046.v1

Pressure was varied in the range of 2.5 – 5.1 MPa to investigate the role of pressure in the fabrication process. We observed that under 3 minutes of pressing time, relatively low temperature of 60°C and a applied pressures of 2.5 and 3.8 MPa, parafilm rarely penetrates into the paper as it cannot be observed at the backside of the paper. With an applied pressure of 5.1 MPa, parafilm slightly permeated through to the back of the device. Nevertheless, a temperature of 80°C and 3 minutes of pressing time enable parafilm to permeate into the paper under applied pressures of 2.5 and 3.8 MPa. However, an applied pressure of 5.1 MPa indicated a slight overflow of parafilm on both the front and back sides. Therefore, the pressure plays a significant role in pushing melted parafilm into the paper matrix.

3.1.3 Effect of pressing time

We investigated the effect of pressing time used in this fabrication in the range of 1 – 5 minutes. At a temperature of 60°C, partially melted parafilm still adheres to the paper under an applied pressure of 2.5 MPa. Even though parafilm does not fully penetrate under this condition, 5 minutes of pressing time are sufficient to push parafilm into the paper matrix, Figure 5a. While a temperature of 80°C successfully melt and push parafilm through the paper in all pressing times from 1 to 5 minutes, Figure 5b. However, a longer pressing time can cause parafilm to over-penetrate and to seep into the pattern. Thus, pressing time also plays a significant role in assisting parafilm to penetrate the paper matrix.

The optimization experiments for parafilm hot pressing were conducted using a patterning mask, with a 5-mm diameter working area. The remaining area is occupied by Parafilm. Therefore, parafilm must be clearly observed on the front and back sides to confirm that it has fully permeated into the paper. The diameter of the hydrophilic area must not be less than 90% from the design. Figure 6 represents the evaluation result, which is labeled with four different colors; red for no parafilm on both sides, orange for parafilm that has not fully permeated, green for parafilm that can be seen on both sides and size larger than 90%, and yellow for over-penetration and size, smaller than 90%. Figure 6 shows that the optimal conditions for the paper-based analytical device used in this study are the temperature at 80°C, pressure at 2.5 - 3.8 MPa, and 3 min of pressing time. In addition, for the manual hot press machine, pressure can be reduced over time due to the restoration of the sample between two pressing plates. Therefore, pressure at 2.5 - 3.8 MPa can successfully push parafilm into the matrix and do not cause over-penetration within 3 minutes of pressing time and at a temperature of 80°C.

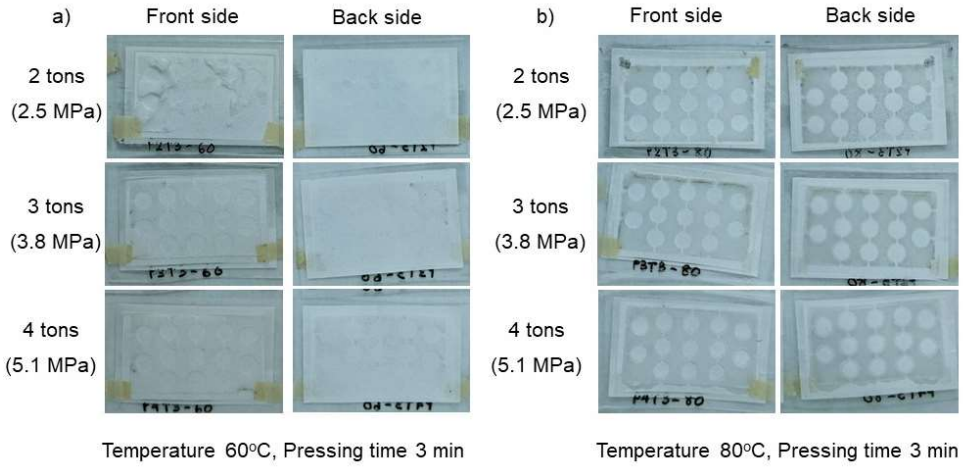

Figure 4 Effect of pressure: (a) Under a temperature of 60 °C and 3 min of pressing time; (b) Under a temperature of 80 °C and 3 min of pressing time. The pressure was varied from 2.5 – 5.1 MPa (2 – 4 tons) in the row (left column shows the front side, right column shows the back side).

Preprints (www.preprints.org) | NOT PEER-REVIEWED | Posted: 3 December 2021 doi:10.20944/preprints202112.0046.v1

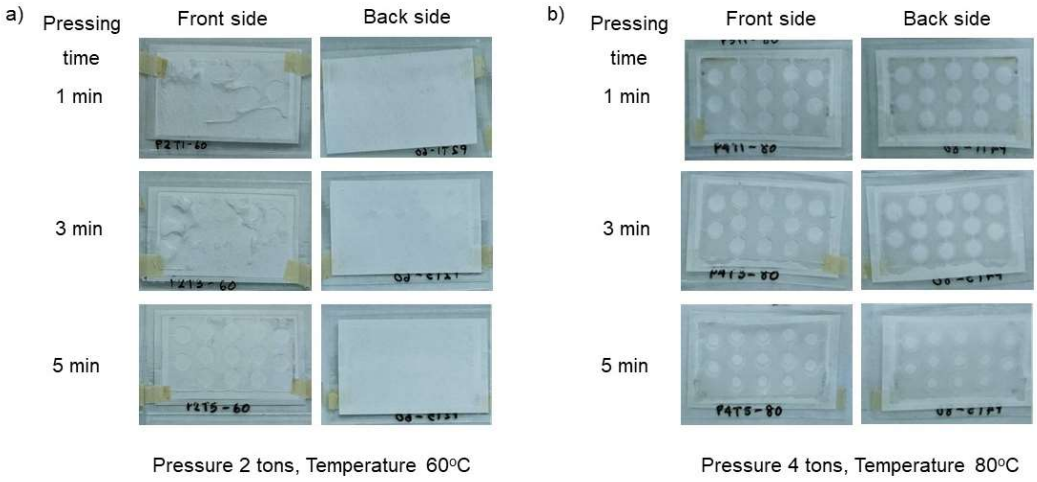

Figure 5 Effect of pressing time: (a) Under a temperature of 60 °C and a pressure of 2.5 MPa (2 tons); (b) Under a temperature of 80 °C and a pressure at 5.1 MPa (4 tons). The pressing time was varied from 1 to 5 min (left column shows the front side, right column shows the back side).

Pressing time (min)

Pressure (MPa)	60°C	1		3		5	
		Front	Back	Front	Back	Front	Back
	2.5 (2 tons)	N/A	N/A	N/A	N/A	89.33%	N/A
	3.8 (3 tons)	N/A	N/A	94.04%	N/A	94.82%	N/A
	5.1 (4 tons)	88.74%	N/A	90.82%	N/A	88.27%	N/A

Pressing time (min)

Pressure (MPa)	70°C	1		3		5	
		Front	Back	Front	Back	Front	Back
	2.5 (2 tons)	91.98%	N/A	91.48%	N/A	92.77%	N/A
	3.8 (3 tons)	92.11%	N/A	94.49%	N/A	93.23%	N/A
	5.1 (4 tons)	92.11%	N/A	93.29%	N/A	90.58%	93.31%

Pressure (MPa)	80°C	1		3		5	
		Front	Back	Front	Back	Front	Back
	2.5 (2 tons)	89.95%	N/A	90.15%	92.11%	90.83%	91.01%
	3.8 (3 tons)	89.01%	90.81%	90.81%	89.04%	76.83%	77.17%
	5.1 (4 tons)	86.88%	83.53%	85.03%	84.98%	59.08%	58.97%

	90°C	1		3		5	
		Front	Back	Front	Back	Front	Back
	2.5 (2 tons)	78.05%	81.02%	67.43%	64.31%	69.43%	65.14%
	3.8 (3 tons)	77.38%	79.30%	58.56%	64.21%	65.66%	64.46%
	5.1 (4 tons)	70.98%	72.25%	70.11%	62.12%	65.87%	63.30%

Figure 6 The evaluation matrix of fabrication parameters determined by the color and percentage of diameter size compared to the design after fabrication. N/A denotes that parafilm cannot be clearly seen at the size and diameter and cannot be measured due to incomplete parafilm permeation. The percentage calculation resulted from the fabricated 5-mm circle with at least three replicates.

3.2 Hydrophobic barrier resolution

The laminate film mask determines the resolution of the fabrication process. As a laser cutting machine uses heat to melt and cut the materials, the smallest size resulting from the cutting mask is the size of the laser point. Figure 7a shows the actual gap from the mask. The gap size of the "No gap" mask was 154 ± 5 μm. In addition, the actual gap of 100 μm, 200 μm, and 300 μm designed masks was 252 ± 25 μm, 346 ± 46 μm, and 455 ± 3 μm, respectively. An explanation is that the increased gap comes from laser melting, Figure 7b.

Preprints (www.preprints.org) | NOT PEER-REVIEWED | Posted: 3 December 2021 doi:10.20944/preprints202112.0046.v1

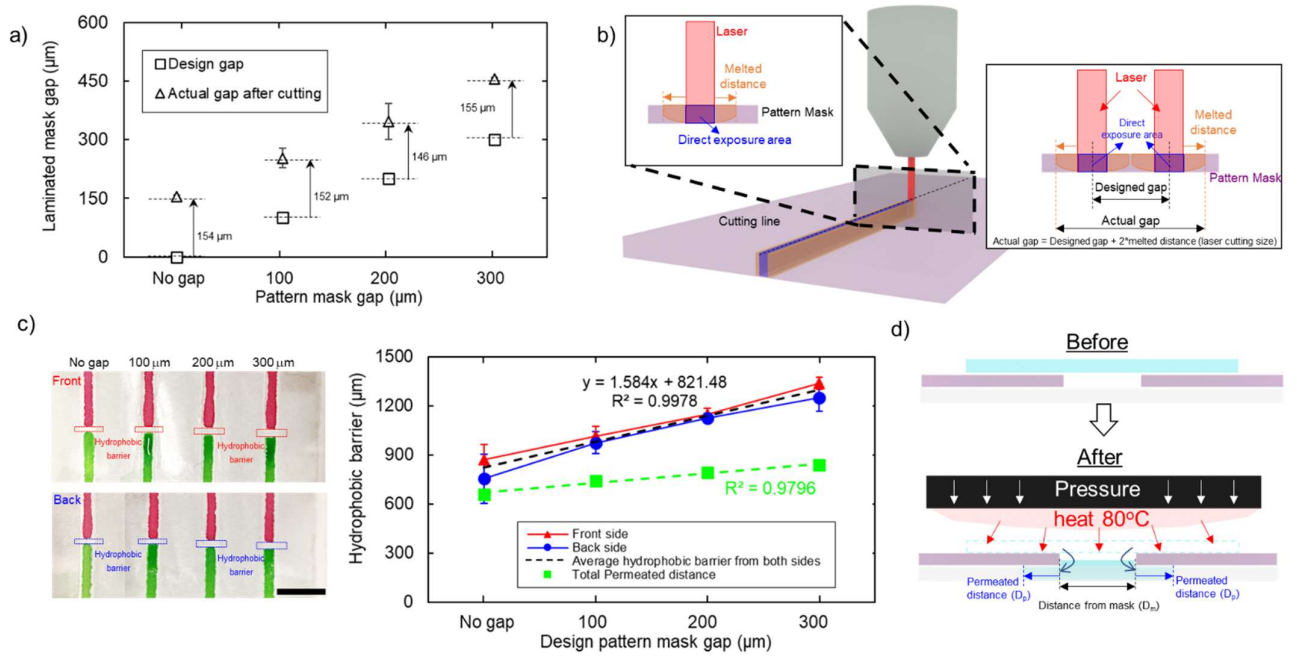

Figure 7 Hydrophobic barrier resolution: (a) The actual gap from laminated mask which was increased approximately 150 μm in all designs, resulting from the laser point size and local laminated mask melting during cutting process; (b) The schematic diagram for laser cutting, showing that the actual gap originating from the laser cutting process is always larger than the designed one; (c) Hydrophobic barrier evaluation and linear relationship between the final hydrophobic barrier with pattern mask, indicating the smallest hydrophobic barrier size from this fabrication is 821.48 μm; (d) Schematic diagram for hydrophobic parafilm melting into the paper showing that melting could be dictated by the distance of the mask (D_m) and permeated distance (D_P).

With the selected fabrication temperature of 80°C, applied pressure at 3.8 MPa and 3 minutes of pressing time, parafilm can penetrate the paper to form a hydrophobic area. Figure 7c illustrates that the hydrophobic barrier on the front side (red markers) is slightly larger than on the backside (blue markers). However, the data between the front and back sides under all conditions are not significantly different ($p < 0.05$). Therefore, we consider that the hydrophobic barrier size used for analysis can be the average of those from the front and back sides. The average hydrophobic barrier size was 813 ± 182 μm, 994 ± 87 μm, 1,137 ± 47 μm and 1,293 ± 89 μm for the actual average gap of 154 μm, 252 μm, 346 μm, and 455 μm, respectively. The parafilm can be melted and dispersed into the paper, which is larger than the actual gap. We found that parafilm dispersal distance results from two parameters which are the patterned mask (D_m) and permeation (D_P). Figure 7d shows that permeation distance (plotted as green markers) are 659 μm, 741 μm, 790 μm, and 838 μm for the actual gap of 120 μm, 252 μm, 346 μm, and 455 μm, respectively, which linearly increased (green dashed line with $R^2 = 0.9796$). The increased permeation of parafilm may result from the presence of additional parafilm between the gap, penetrating into the paper.

As a result, we found a linear relationship between the designed gap (in micrometers for the x-axis and hydrophobic barrier size in micrometers for the y-axis) with the trend line of $y = 1.584x + 821.48$ ($R^2 = 0.9978$) as shown in Figure 7c. This equation can be used to estimate the hydrophobic barrier size corresponding to the designed pattern. This relationship includes the effect of the laminated mask and the permeation of parafilm in the fabrication. The smallest hydrophobic barrier structure can be formed with this method is 821 μm, which is a similar result for the case of no gap in the designed mask.

3.3 Physical and biochemical properties of the paper

3.3.1 Flowing characteristics

 doi:10.20944/preprints202112.0046.v1

We investigated the wicking mechanism to evaluate the physical properties of the paper after fabrication. We observed wicking in the paper strip and plotted the relationship between the distance of the liquid front versus the square root of time. Figure 8a indicates that the fabricated paper results in a slightly smaller slope than the original paper (1.45 – 1.58 for fabricated paper vs 1.78 – 1.79 for original paper). According to the Washburn's relationship, the slope between the distance of the liquid front and the square root of time is proportional to the pore size of the paper matrix [26]. A lower slope may originate from the smaller pore size resulting from pressure in the fabrication process [27]. However, the wicking mechanism still follows the conventional Washburn relationship with R-square (0.974 – 0.986 for fabricated paper vs 0.980 – 0.990 for original paper). Moreover, the lower wicking speed may also enhance sensitivity, allowing more time for a reaction to occur and better results. Consequently, longer fluid wicking in an open environment may encounter evaporation issues [28,29]. Therefore, the pressure and heat from the fabrication process may affect the wicking mechanism by slightly decreasing the wicking speed, but it does not break the Washburn relationship.

3.3.2 Colorimetric sandwich immunological assay

We perfomed a colorimetric sandwich immunological assay to evaluate protein binding on the paper matrix after hot pressing fabrication, Figure 8b. The image was processed and quantified as per the bar diagram shown in Figure 8b. The result showed that in the presence of rabbit anti-human CD9, goat anti-rabbit IgG conjugated with HRP would be captured resulting from the immunoaffinity interaction, subsequently reacting with TMB, resulting in the development of a blue-colored charge transfer complex due to HRP/TMB reaction. While in the absence of rabbit anti-human CD9, goat anti-rabbit IgG conjugated with HRP would be absent due to the lack of an immunoaffinity interaction, remaining as a colorless solution. However, a slight blue color may be presented due to non-specific adsorption. Blue color development at the 20th minute in the presence of rabbit anti-human CD9 (grey bar in Figure 8b) was slightly higher than that of original paper (white bar in Figure 8b). Under the same conditions, TMB solution remains on the fabricated paper as seen by the light reflection in the light box. In contrast, on original paper, there is no leftover liquid form of TMB solution. Heat and pressure resulting from fabrication may result from the smaller pore size of the paper as a result of more reaction time leading to more blue intensity [29]. This observation corresponds to the wicking experiment in the previous section showing that wicking in the fabricated paper strip is slightly slower than in original paper. As demonstrated by the TMB/HRP reaction, the immunological assay can be performed with the hot-press fabricated paper.

3.4 2D and 3D paperfluidic applications

We performed mixing experiments in 2D paperfluidic devices and 3D paperfluidic channels was performed to demonstrate the 2D and 3D paperfluidic applications. For mixing in 2D paperfluidic devices, 0.1M NaOH and phenolphthalein pH indicator were dropped at the inlets for interaction in the straight channel shown in Figure 9a. The color changed from colorless to pink, showing that the chemical reaction can take place in over 0 to 200 seconds in our paper device. The paper-based device made with our method is compatible with 2D mixing. Moreover, we implemented a 3D paperfluidic channel, as shown in Figure 9b. The liquid can independently flow in its 3D channel without mixing with other channels as the same color can be seen from its reservoir to the end of the channel. As a result, the paper-based device (fabricated layer-by-layer and assembled to create 3D paperfluidics) was successfully demonstrated. Therefore, parafilm hot pressing fabrication has a great potential to be applicable to more complex analytical applications in both 2D and 3D configurations.

Preprints (www.preprints.org) | NOT PEER-REVIEWED | Posted: 3 December 2021 doi:10.20944/preprints202112.0046.v1

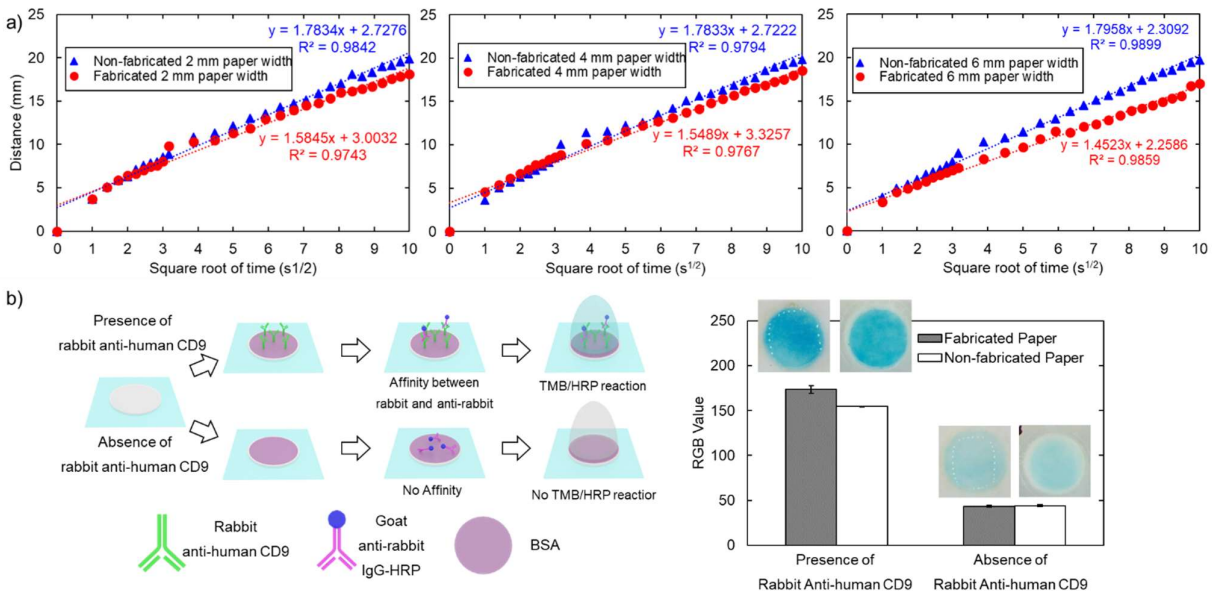

Figure 8 Physical and biochemical properties of the paper: (a) Flow characteristics resulting from 2-mm, 4-mm and 6-mm paper strips. A blue marker for original paper and a red marker for fabricated paper; (b) Schematic diagram for colorimetric immunological assay in the presence and absence of rabbit anti-human CD9 with the bar diagram for RGB_{value} quantified at the 20^{th} minute of the TMB/HRP assay with MATLAB between fabricated (grey bar) and non-fabricated paper (white bar). Error bars represent the standard deviation from the average of three replicates ($n = 3$).

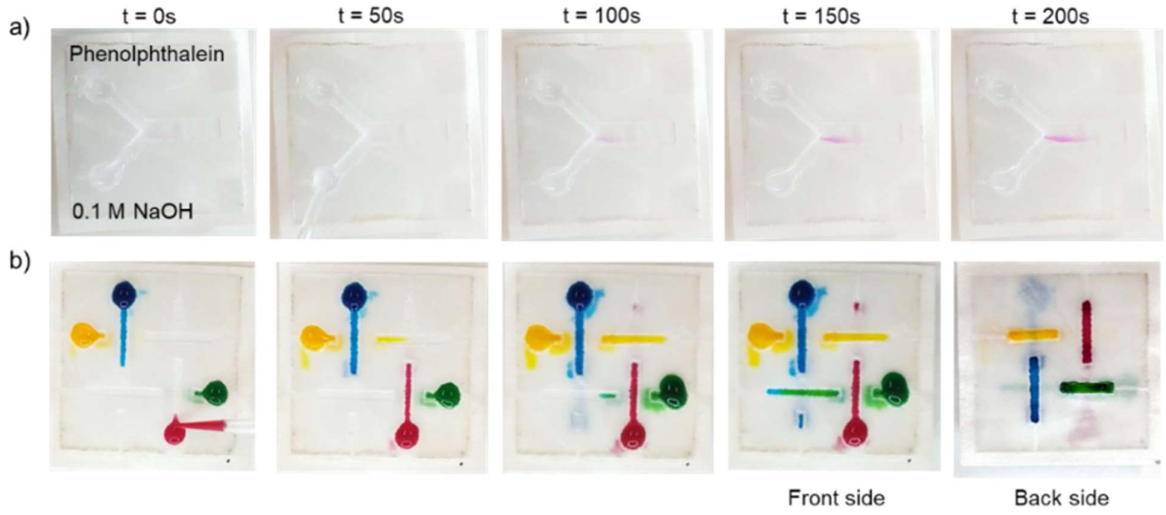

Figure 9 Analytical assay test: (a) Mixing between 0.1 M NaOH and phenolphthalein pH indicator in the 2D analytical paper-based device; (b) Flow in the 3D configuration paper-based device showing that there was no mixture of color as shown in the final front and back side of the paper device.

4. Conclusion

In conclusion, we have successfully fabricated paper-based analytical devices using parafilm hot pressing. The paper-based fabrication conducted in this study offered (i) spped with the whole process occurring within 5 - 10 minutes, (ii) simplicity which included only two steps: cutting the mask with a laser cutting machine and hot pressing, and (iii) low cost with the total fabrication cost being less than 0.01 USD. We studied the effect of three fabrication parameters: pressure, temperature, and pressing time. The optimized conditions for the fabrication include pressure of 3.8 MPa, temperature of 80°C, and

time of 3 minutes, with the determination of the equation of the approximate hydrophobic barrier size from the design of the mask gap. The smallest hydrophobic barrier resulting from the laminated mask and melting parafilm in the fabrication is 821 μm. We also investigated the physical and biochemical properties of the paper-based device after the fabrication to affirm the functionality of the paper for analytical devices. In addition, we successfully demonstrated mixing for 2D and 3D paperfluidic applications. We believe that parafilm hot pressing techniques have the potential for scaling up in mass production due to its rapid, simple, and inexpensive nature.

Author Contributions: Conceptualization, S.K. and N.T.N.; methodology, S.K. and K.C.; validation, S.K., K.C., M.J.A.S and N.T.N.; data curation, S.K. and K.C.; writing—original draft preparation, S.K., K.C., M.J.A.S and N.T.N.; writing—review and editing, S.K., K.C., M.J.A.S and N.T.N.; supervision, M.J.A.S and N.T.N.

Acknowledgments: The authors acknowledge the support of the Australian Research Council (DP180100055) and higher degree research scholarships GUIPRS and GUPRS Scholarships to S.K. from the Griffith University.

Conflicts of Interest: The authors declare no conflict of interest.

References

1. Martinez, A.W.; Phillips, S.T.; Whitesides, G.M.; Carrilho, E. Diagnostics for the Developing World: Microfluidic Paper-Based Analytical Devices. *Analytical Chemistry* **2010**, *82*, 3-10, doi:10.1021/ac9013989.
2. Cate, D.M.; Adkins, J.A.; Mettakoonpitak, J.; Henry, C.S. Recent Developments in Paper-Based Microfluidic Devices. *Analytical Chemistry* **2015**, *87*, 19-41, doi:10.1021/ac503968p.
3. Yetisen, A.K.; Akram, M.S.; Lowe, C.R. Paper-based microfluidic point-of-care diagnostic devices. *Lab on a Chip* **2013**, *13*, 2210-2251, doi:10.1039/C3LC50169H.
4. Martinez, A.W.; Phillips, S.T.; Whitesides, G.M. Three-dimensional microfluidic devices fabricated in layered paper and tape. *Proceedings of the National Academy of Sciences* **2008**, *105*, 19606, doi:10.1073/pnas.0810903105.
5. Akyazi, T.; Basabe-Desmonts, L.; Benito-Lopez, F. Review on microfluidic paper-based analytical devices towards commercialisation. *Analytica Chimica Acta* **2018**, *1001*, 1-17, doi:https://doi.org/10.1016/j.aca.2017.11.010.
6. Lisowski, P.; Zarzycki, P.K. Microfluidic Paper-Based Analytical Devices (μPADs) and Micro Total Analysis Systems (μTAS): Development, Applications and Future Trends. *Chromatographia* **2013**, *76*, 1201-1214, doi:10.1007/s10337-013-2413-y.
7. Martinez, A.W.; Phillips, S.T.; Butte, M.J.; Whitesides, G.M. Patterned Paper as a Platform for Inexpensive, Low-Volume, Portable Bioassays. *Angewandte Chemie International Edition* **2007**, *46*, 1318-1320, doi:https://doi.org/10.1002/anie.200603817.
8. Martinez, A.W.; Phillips, S.T.; Wiley, B.J.; Gupta, M.; Whitesides, G.M. FLASH: A rapid method for prototyping paper-based microfluidic devices. *Lab on a Chip* **2008**, *8*, 2146-2150, doi:10.1039/B811135A.
9. Bruzewicz, D.A.; Reches, M.; Whitesides, G.M. Low-Cost Printing of Poly(dimethylsiloxane) Barriers To Define Microchannels in Paper. *Analytical Chemistry* **2008**, *80*, 3387-3392, doi:10.1021/ac702605a.
10. Lu, Y.; Shi, W.; Jiang, L.; Qin, J.; Lin, B. Rapid prototyping of paper-based microfluidics with wax for low-cost, portable bioassay. *ELECTROPHORESIS* **2009**, *30*, 1497-1500, doi:https://doi.org/10.1002/elps.200800563.
11. Li, X.; Tian, J.; Garnier, G.; Shen, W. Fabrication of paper-based microfluidic sensors by printing. *Colloids and Surfaces B: Biointerfaces* **2010**, *76*, 564-570, doi:https://doi.org/10.1016/j.colsurfb.2009.12.023.
12. Olkkonen, J.; Lehtinen, K.; Erho, T. Flexographically Printed Fluidic Structures in Paper. *Analytical Chemistry* **2010**, *82*, 10246-10250, doi:10.1021/ac1027066.
13. Sun, J.-Y.; Cheng, C.-M.; Liao, Y.-C. Screen Printed Paper-based Diagnostic Devices with Polymeric Inks. *Analytical Sciences* **2015**, *31*, 145-151, doi:10.2116/analsci.31.145.

14. Songjaroen, T.; Dungchai, W.; Chailapakul, O.; Laiwattanapaisal, W. Novel, simple and low-cost alternative method for fabrication of paper-based microfluidics by wax dipping. *Talanta* **2011**, *85*, 2587-2593, doi:https://doi.org/10.1016/j.talanta.2011.08.024.
15. Abe, K.; Suzuki, K.; Citterio, D. Inkjet-Printed Microfluidic Multianalyte Chemical Sensing Paper. *Analytical Chemistry* **2008**, *80*, 6928-6934, doi:10.1021/ac800604v.
16. Li, X.; Tian, J.; Nguyen, T.; Shen, W. Paper-Based Microfluidic Devices by Plasma Treatment. *Analytical Chemistry* **2008**, *80*, 9131-9134, doi:10.1021/ac801729t.
17. Cai, L.; Xu, C.; Lin, S.; Luo, J.; Wu, M.; Yang, F. A simple paper-based sensor fabricated by selective wet etching of silanized filter paper using a paper mask. *Biomicrofluidics* **2014**, *8*, 056504-056504, doi:10.1063/1.4898096.
18. Chitnis, G.; Ding, Z.; Chang, C.-L.; Savran, C.A.; Ziaie, B. Laser-treated hydrophobic paper: an inexpensive microfluidic platform. *Lab on a Chip* **2011**, *11*, 1161-1165, doi:10.1039/C0LC00512F.
19. Kim, Y.S.; Yang, Y.; Henry, C.S. Laminated and infused Parafilm® - paper for paper-based analytical devices. *Sens Actuators B Chem* **2018**, *255*, 3654-3661, doi:10.1016/j.snb.2017.10.005.
20. Xia, Y.; Si, J.; Li, Z. Fabrication techniques for microfluidic paper-based analytical devices and their applications for biological testing: A review. *Biosensors and Bioelectronics* **2016**, *77*, 774-789, doi:https://doi.org/10.1016/j.bios.2015.10.032.
21. Lim, H.; Jafry, A.T.; Lee, J. Fabrication, Flow Control, and Applications of Microfluidic Paper-Based Analytical Devices. *Molecules* **2019**, *24*, doi:10.3390/molecules24162869.
22. Dunfield, E.M.; Wu, Y.Y.; Remcho, T.P.; Koesdjojo, M.T.; Remcho, V.T. Simple and rapid fabrication of paper microfluidic devices utilizing Parafilm®. **2012**.
23. Yu, L.; Shi, Z.Z. Microfluidic paper-based analytical devices fabricated by low-cost photolithography and embossing of Parafilm®. *Lab on a Chip* **2015**, *15*, 1642-1645, doi:10.1039/C5LC00044K.
24. Kasetsirikul, S.; Shiddiky, M.J.A.; Nguyen, N.-T. Wicking in Paper Strips under Consideration of Liquid Absorption Capacity. *Chemosensors* **2020**, *8*, doi:10.3390/chemosensors8030065.
25. Kasetsirikul, S.; Umer, M.; Soda, N.; Sreejith, K.R.; Shiddiky, M.J.A.; Nguyen, N.-T. Detection of the SARS-CoV-2 humanized antibody with paper-based ELISA. *Analyst* **2020**, *145*, 7680-7686, doi:10.1039/D0AN01609H.
26. Washburn, E.W. The Dynamics of Capillary Flow. *Physical Review* **1921**, *17*, 273-283, doi:10.1103/PhysRev.17.273.
27. Shin, J.H.; Park, J.; Kim, S.H.; Park, J.-K. Programmed sample delivery on a pressurized paper. *Biomicrofluidics* **2014**, *8*, 054121-054121, doi:10.1063/1.4899773.
28. Park, J.; Shin, J.H.; Park, J.-K. Pressed Paper-Based Dipstick for Detection of Foodborne Pathogens with Multistep Reactions. *Analytical Chemistry* **2016**, *88*, 3781-3788, doi:10.1021/acs.analchem.5b04743.
29. Mao, X.; Ma, Y.; Zhang, A.; Zhang, L.; Zeng, L.; Liu, G. Disposable Nucleic Acid Biosensors Based on Gold Nanoparticle Probes and Lateral Flow Strip. *Analytical Chemistry* **2009**, *81*, 1660-1668, doi:10.1021/ac8024653.